European Journal of Pharmaceutical Sciences 193 (2024) 106671

Contents lists available at ScienceDirect

European Journal of Pharmaceutical Sciences

journal homepage: www.elsevier.com/locate/ejps

^{18}F-labeled somatostatin analogs for somatostatin receptors (SSTRs) targeted PET imaging of neuroendocrine tumors (NETs)

Fei Gao [a,1], Yunhan Zhang [a,b,1], MengYi Chen [a], ZhiHao Song [a], RuiLin Dong [a], ShanShan Qiu [a], Chen Shen [a], XiaoYan Huang [a], Hao Geng [a], Weihua Cheng [a,*], Ji Hu [a,*]

[a] HTA Co., Ltd., CAEA Center of Excellence on Nuclear Technology Applications for Engineering and Industrialization of Radiopharmaceuticals, CNNC Engineering Research Center of Radiopharmaceuticals, Beijing, China

[b] Biomedical Engineering Department, Huazhong University of Science and Technology, Wuhan, China

ARTICLE INFO

Keywords:
Neuroendocrine tumors (NETs)
Somatostatin receptor (SSTR)
Fluorine-18-labeled PET tracer
Al^{18}F · PET/CT
Somatostatin analogue

ABSTRACT

Purpose: A novel ^{18}F-radiolabeled somatostatin analogue, [Al^{18}F]NODA-MPAA-HTA, was synthesized and evaluated for positron emission tomography (PET) imaging of Neuroendocrine tumors (NETs). [Al^{18}F]NODA-MPAA-HTA was designed and synthesized by conjugating ^{18}F nuclide with a modified KE108 peptide, a somatostatin analog with high affinity for all five subtypes of somatostatin receptors (SSTR 1–5), through coupling a bifunctional chelator (NODA) to target somatostatin receptor (SSTR) positive tumors.

Methods: The amino group of KE108 peptide, a SSTRs-targeting pharmacophore, was conjugated with the carboxyl group of NODA by a condensation reaction to obtain the labeling precursor of [Al^{18}F]NODA-MPAA-HTA, in which its precursor was obtained through Fmoc solid-phase methods. A novel methodology for Al^{18}F labeling of chelating agent-biomolecule conjugates was used to synthesize [Al^{18}F]NODA-MPAA-HTA. In *vitro* stabilities of [Al^{18}F]NODA-MPAA-HTA were evaluated by incubating it in saline or bovine serum for 2 h. *Ex vivo* biodistribution and in vivo imaging of [Al^{18}F]NODA-MPAA-HTA were further investigated to evaluate its SSTRs targeting ability and feasibility for the diagnosis of NETs using PET imaging.

Results: [Al^{18}F]NODA-MPAA-HTA was synthesized using a one-step ^{18}F-AlF labeling procedure resulting in moderate radiochemical yield (60–80 %, non-decay corrected) and high radiochemical purity (>95 %). It exhibited good hydrophilicity and excellent stability in vitro, with a molar activity of 122 GBq/μmol. At 30 min and 60 min, the uptake of [Al^{18}F] NODA-MPAA-HTA by HEK293-SSTR2 cells was 5.47 ± 0.97 %/105 cells and 12.11 ± 0.32 %/105 cells, respectively. The affinity of [Al^{18}F]NODA-MPAA-HTA for SSTR2 was determined to be 8.77 ± 1.14 nM. In micro-PET imaging of HEK293-SSTR2 tumor-bearing mice, [Al^{18}F]NODA-MPAA-HTA showed high tumor uptake of radioactivity and a high tumor-to-muscle ratio. Biodistribution results confirmed that radioactivity uptake in the tumor was significantly higher than that in the muscle by more than five-fold ($P<0.001$). Furthermore, the relatively low bone uptake of [Al^{18}F]NODA-MPAA-HTA suggested that defluorination did not occur in vivo. These preliminary results provide experimental evidence for further study of Al^{18}F-labeled somatostatin analogues as tumor probes for PET imaging of NETs.

Conclusion: Fluorine-18 is widely used as a radionuclide for the production of radiopharmaceuticals for positron emission tomography (PET). Due to its short half-life (T1/2,109.8 min), its ease of production will facilitate the widespread dissemination of this radiopharmaceutical. A high-quality [Al^{18}F]NODA-MPAA-HTA was synthesized with satisfactory yield. This radiopharmaceutical demonstrated higher tumor uptake and better tumor-to-muscle contrast, resulting to excellent image quality. These findings suggest that the novel ^{18}F-labeled somatostatin analogue, [Al^{18}F]NODA-MPAA-HTA, is a promising tool for PET imaging of NETs.

* Corresponding authors.
E-mail addresses: chengweihua@circ.com.cn (W. Cheng), huji@circ.com.cn (J. Hu).

[1] Fei Gao and Yunhan Zhang contributed equally to this work.

https://doi.org/10.1016/j.ejps.2023.106671
Received 19 July 2023; Received in revised form 8 December 2023; Accepted 11 December 2023
Available online 16 December 2023

1. Introduction

Neuroendocrine tumors (NETs) are a heterogeneous malignant disease that can originate from different neuroendocrine organs and can develop anywhere in the body, especially due to its rare and a wide range of clinical behaviors (Turaga and Kvols, 2011; Yao et al., 2008). Over the years, traditional medical imaging techniques (CT, MR, ultrasound) have played an important role in achieving early diagnosis and precise treatment of malignant tumors through anatomical imaging in medical imaging for diagnosis, surgical guidance, follow-up, and treatment monitoring. However, the rapid development of molecular imaging (PET and SPECT) has higher sensitivity and specificity, and the rapid development in combination with CT or MRI has been used in the diagnosis, staging and treatment of various malignant tumors. Due to the diversity and non-specificity of early NETs symptoms, diagnosing the disease can be challenging for doctors, causing patients with NETs to suffer delays in diagnosis for many years (Dasari et al., 2017). In the process of metastatic disease progression, the combination of slow progression and hormone secretion may produce weakened symptoms and may have more serious effects, leading to deterioration of quality of life and consumption of medical resources. Over the past few decades, the incidence of neuroendocrine tumors has witnessed a substantial increase (Kourie, 2016; Toshihiko et al., 2020; Hallet et al., 2015). The hypothesis of sensitivity of detection instruments or changes in tumor biology has been used to explain this observation, but currently there is no data to support these two hypotheses. The reasons underlying of the increase in the incidence rate of NETs have not been identified, although it has been reported globally (Hallet et al., 2015). Research has demonstrated the critical role of somatostatin receptors (SSTR), which encompass five subtypes in targeting NETs (Kaemmerer et al., 2011; Modlin et al., 2010), with SSTR2 being the most predominant one (Reubi and Maecke, 2008). Therefore, radiolabeled SSTR analogues can effectively target and visualize NETs in vivo. These analogues can be utilized in both SPECT/CT and PET/CT imaging, allowing for accurate diagnosis and staging of NETs.

So far, several radiolabeled SSTR-targeted probes have been reported and evaluated for imaging and therapy of SSTR2-overexpressing neuroendocrine tumors. These include ^{68}Ga-DOTA-conjugated peptides (^{68}Ga-dotatate (Kaemmerer et al., 2011; Modlin et al., 2010), ^{68}Ga-dotatoc (Hofmann et al., 2001; Loft et al., 2017), ^{68}Ga-dotanoc (Kaemmerer et al., 2011; Campana et al., 2010)), ^{177}Lu-dotatate (Strosberg et al., 2017; Kobayashi et al., 2021; Capello et al., 2003), ^{64}Cu-dotatate (Loft et al., 2017) and some octreotide derivatives (Cai et al., 2014; Lewis et al., 1999), as well as other radioactive SSTR derivatives (Modlin et al., 2010; Kunikowska et al., 2011; Eisenwiener et al., 2002) and imaging agents (Kjaer and Knigge, 2015) Somatostatin-derived tracers have undergone nearly 35 years of successful development and extensive clinical applications. Among the radiolabeled SSTR-targeted probes, ^{68}Ga-dotatate and ^{177}Lu-dotatate have gained significant attention, particularly for their application in molecular imaging and targeted radionuclide therapy in nuclear oncology. Although ^{68}Ga and ^{64}Cu labeled somatostatin analog radiotracers has demonstrated promising clinical utility, the widespread adoption is impeded by the substantial cost and limited supply of these radionuclides.

In contrast to ^{68}Ga, ^{18}F is one of the favored radionuclides because of its longer half-life and higher production yield, which facilitates centralized and distributed manufacturing. This allows for the accommodation of a larger population of patients, making ^{18}F-labeled radiotracers more accessible for diagnostic purposes in the management of neuroendocrine tumors (Chen et al., 2016). Additionally, ^{18}F has excellent imaging characteristics including a high positron emission yield (97 % β+), energy (0.64 MeV), and a relatively short half-life (109.8 min), the shorter positron range of ^{18}F enables higher-resolution PET imaging and quantification of biochemical processes in vivo. Considering these advantages, several promising ^{18}F-based tracers targeting the somatostatin receptor have emerged (Leupe et al., 2023). These radioactive probes can be used for diagnosing and staging diseases, as well as to predict and/or monitor response to therapy. For example, [^{18}F]AlF-NOTA-octreotide had been applied in clinical studies and been provided with good imaging ability, especially for liver tumor imaging. In addition, [^{18}F]AlF-NOTA-JR11 also showed lower physiological uptake in the digestive system compared to ^{68}Ga-dotatate. As reported, ^{68}Ga-dotatate and ^{177}Lu-dotatate mainly target NETs of the subtypes 2 and 5. As a somatostatin analogue with high affinity for all five SSTR subtypes, KE108 exhibits a similar chemical structure to octreotide but possesses a broader spectrum for SSTR-positive tumors. The radiolabeling technology known as "^{18}F-AlF" has the advantages of one-step reaction and radioactive labeling in water, rendering it a convenient and efficient method for radiolabeling. The novel methodology for ^{18}F labeling of chelating agent-biomolecule conjugates was based on unusually strong and stable fluoro bond between Al^{3+} and fluoride which bond dissociation energy was 675 kJ/mol (Kumar, 2018; Martell, 1996; André et al., 2002). This technology has been successfully applied in previous research (Kumar, 2018; Malik et al., 2015) due to the tendency of carboxylate to form thermodynamically stable (Edit et al., 2015) and kinetically inert metal chelates. Chelated pan-somatostatin ligands (NOTA, DOTA, etc.) play an important role in the development of potential targets for a wider range of tumors (Wild et al., 2003; Ginj et al., 2008). The application of ^{18}F-peptide labeling method coupled with bifunctional chelating agents has greatly advanced the development of ^{18}F labeled peptide positron drugs (Kumar, 2018; Mcbride et al., 2010). Compared with existing methods or techniques for similar syntheses and radiolabeling, this his method is characterized by its simplicity, speed, one-pot synthesis and ability to accomplish the labeling of ^{18}F nuclides in an aqueous environment, making it a valuable tool for the development of novel radiotracers for diagnosing and managing various diseases, including neuroendocrine tumors.

In this study, we designed and synthesized a novel probe that targets SSTRs through a one-step ^{18}F-AlF labeling method, which yielded a ^{18}F-labeled radiotracer ([Al^{18}F]NODA-MPAA-HTA) by conjugating with a bifunctional chelator (NODA). We evaluated this probe both in vitro and in vivo, assessing its physical and chemical properties, PET imaging ability, and biodistribution in tumor-bearing mice using micro-PET/CT to verify its tumor targeting capability.

2. Experimental section

2.1. General

Unless noted otherwise, all reagents used were commercially purchased. ECLIPSE HP cyclotron (Siemens, Germany), Electrospray ionization mass spectrometry (Waters, ESI-MS, SYNAPT G2 HDMS) data were obtained using a mass spectrometer (Waters, USA). An HPLC system (CBN-20, Shimadzu, Japan) equipped with a UV detector and a radioactive detector (GABI, Raytest, Germany) separated by a C-18 column (Agilent ZORBAX XDB-C18, 5 μm, 4.6 × 250 mm).

SSTR2(+) HEK293-SSTR2 cells (Ubigene Biosciences Co., Ltd., Guangzhou, China) were cultured in a 24-well plate and cultured in DMEM medium, which was grown as a monolayer at 37 °C in a moist atmosphere of 5 % CO_2. The Healthy BALB/c mice and tumor model mice were approved by the guide for the care and use of institutional animal of Institute of Medicinal Biotechnology (No. IMB20220516D7).

2.2. Radiochemistry

The synthesis route of [Al^{18}F]NODA-MPAA-HTA were shown in Scheme 1. NODA-MPAA-HTA peptide served as a model substrate to optimize the labeling conditions. Approximately 3.7 GBq [^{18}F]F^- (Cyclone 30, IBA, Belgium) was captured with a QMA SepPak light cartridge (Waters) activated with 10 mL of metal-free water. [^{18}F]F^-

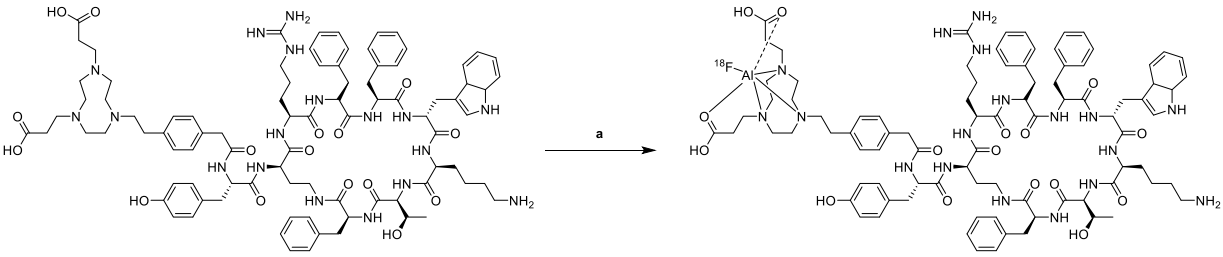

Scheme 1. Synthesis route of [Al^{18}F]NODA-MPAA-HTA.
Reagents and conditions: (a) NODA-MPAA-HTA peptide, acetic acid buffer, gentianic acid, $AlCl_3$, anhydrous acetonitrile, 110 °C, 20 min.

was eluted by 0.5 mL of 0.9 % NaCl from a QMA column, and 100 μL of (0.74 GBq). [^{18}F]F^- was added to the reaction vial. Before adding [^{18}F]F^-, 50 μL of peptide solution (1 mg/mL in metal-free water), the proper volumes of $AlCl_3$ (2 mM in 0.1 M acetate buffer), 100 μL of acetate buffer, and 100 μL of acetonitrile were added. 10 μL of gentisic acid (10 mg/mL) was added to the reaction to reduce radiolysis. The optimal preparation conditions were selected by determining the radiochemical yields under different conditions of $AlCl_3$ solution dosage, pH, temperature and reaction time in the reaction system.

After cooling, the reaction liquid was applied to a C18 SepPak light cartridge proactivated by 10 mL of ethanol and 10 mL of water, which was eluted the free [^{18}F]F^- or [^{18}F]AlF_2^-. Subsequently, [Al^{18}F]NODA-MPAA-HTA was eluted by 0.5 mL of 50 % (v/v) ethanol and diluted with 0.9 % NaCl. A typical HPLC analytic gradient was 30 %−65 % B (contained 0.1 % (v/v) TFA in water) over 10 min, 65 %−35 % B in 10–15 min, at a flow of 1 mL/min.

2.3. Pharmacokinetics

[Al^{18}F]NODA-MPAA-HTA was injected into healthy BALB/c mice via their tail veins at 3.7 MBq (100 μCi)/125 μL/head ($n = 3$). Blood samples were collected from the retroorbital plexus into capillary at 5, 10, 15, 30, 60 and 120 min. The radioactivity of blood samples was evaluated and calculated as %ID/g (percentage of injected dose per gram of tissue) by a γ-counter (Perkinelmer Wallac). Radioactive counts in blood samples are measured by physical decay correction. Using Drug and Statistics for Windows 2.0 software (DAS, Cary, NC), pharmacokinetic parameters were calculated using statistical moment method using a noncompartment model. Non-compartmental models typically use statistical moment parameters which do not require that the drug process in vivo to conform to linear kinetics, rather than setting up specific compartments. It is suitable for tracer kinetic analysis where the existing knowledge is insufficient to set up the compartment model, or the sample collection cannot meet the requirements of compartment model analysis.

Non-compartmental models, characterized by statistical moment parameters, are advantageous as they treat the in vivo drug process as a global effect of the stochastic process of drug molecules with varying residence times in the body. These models describe the in vivo drug process solely based on the area under the concentration-time curve (AUC), thereby obviating the need for predefined compartments.

2.4. Saturation cell binding and cellular uptake

The competitive cell binding assays were performed as described previously (Chen et al., 2021). SSTR2(+) HEK293-SSTR2 cells (10^5 cells/well) were cultured in a 24-well plate and incubated with [Al^{18}F]NODA-MPAA-HTA in the presence of 8 different concentrations of NODA-MPAA-HTA peptide (0 - 100 nM, 250 μL/well) for 1 h at 37 °C. To determine the non-specific uptake, excessive NODA-MPAA-HTA peptide (20 μL per well, 1 mg/mL) was added additionally to the cells prior to the incubation with radiotracer on another 24-well plate. After incubation, the cells were washed 2 times with PBS (0.01 M) and collected after digestion with 1 M NaOH ($n = 4$). Cell-bound radioactivity was measured with a γ-counter. Specific binding is obtained by subtracting non-specific binding from total binding, and performing nonlinear regression fitting on specific binding values at different concentrations. The value of K_d (ligand concentration that binds to half the receptor sites at equilibrium) and B_{max} (maximum number of binding sites) were calculated by fitting the data with a nonlinear regression algorithm (GraphPad Prism 5.0 software). K_d and B_{max} were calculated using the following equation: $Y = B_{max}*X/(K_d+X)$.

For the determination of specific cellular uptake, SSTR2(+) HEK293-SSTR2 cells seeded in 24-well plates (10^5 cells /well) were incubated for 24 h. Then they were washed twice with 1 mL PBS and incubated with or without NODA-MPAA-HTA peptide (250 μL / well, 0.3 mg/mL) for 1 h. [Al^{18}F]NODA-MPAA-HTA was added and then the cells were incubated at 37 °C for 0.5, 1 and 2 h. After that, the cells were washed twice with 1 mL of PBS and lysed with 1 mL of NaOH (1 mol/L), and the cell extract was collected using a γ-counter.

2.5. PET imaging studies

According to the literature (Xie et al., 2021),receptor-specific uptake was determined using nude mice bearing HEK293-SSTR2 tumor. Small-animal PET/CT images were performed after [Al^{18}F]NODA-MPAA-HTA (3–5 MBq/125 μL) was administered intravenously to the HEK293-SSTR2 tumor-bearing mice. A 10 min PET scan performed for attenuation correction was performed on a β-CUBE scanner (MOLECUBES, Ghent, Belguim), followed by a 5 min CT scan on an X-CUBE scanner (MOLECUBES, Ghent, Belguim) under anesthesia using isoflurane. The mice were anesthetized using isoflurane/O_2, and their body temperature was kept constant with an integrated heating circuit. PET images were acquired at 0.5, 1, and 2 h post-injection time (p.i.). All PET data were reconstructed by three-dimensional orderedsubset expectation maximization (16 subsets, 2 iterations) with attenuation and scatter correction. CT images were subsequently acquired using a helical scan with the following acquisition parameters: an X-ray source setting of 50 kVp/100 μA, 480 projections, a 1.4 spiral pitch, resulting in a 3 min acquisition time. Image analysis was performed using the VivoQuant software (version 4.0 patch1, inviCRO, LLC, Boston, MA, USA).

2.6. Biodistribution of [Al^{18}F]NODA-MPAA-HTA

The biodistribution study was adopted in nude mice bearing HEK293-SSTR2 tumor to further reveal the absolute tracer uptake in the tissues of interest. The [Al^{18}F]NODA-MPAA-HTA (0.37 MBq/100 μL) was injected into mice ($n = 4$ each group) via the tail vein, and the mice were sacrificed at 0.5, 1 and 2 h p.i.. The muscle of the contralateral hind limb of the mouse was selected in biodistribution study. And the tissues of interest were sampled and weighed, and counted separately using a γ-counter.

3. Statistical and data analysis

Data were expressed as mean ± SD and the significance of

comparison between two data sets was determined using SPSS 20.0 statistical software and defined as significant (*$P < 0.05$).

4. Results

4.1. Chemical and radiochemical syntheses

We designed and synthesized the precursor, NODA-MPAA-HTA, which was obtained through Fmoc solid-phase synthesis via the condensation reaction and cyclization reaction between multiple amino acids, followed by the introduction of the bifunctional chelator (NODA). The labeling precursor was obtained (Supplemental Scheme 1) with 95 % chemical purity and identified using mass spectrometry (Supplemental Fig. 1).

The radiosynthesis of [Al^{18}F]NODA-MPAA-HTA was achieved by a novel ^{18}F labeling methodology for chelating agent-biomolecule conjugates (McBride et al., 2009). [Al^{18}F]NODA-MPAA-HTA was radiolabeled via the complexation of Al^{18}F by the NODA chelator according to Scheme 1. Remarkably, even at low peptide concentrations 30 nmol (50 μL, 1 mg/mL), we were able to successfully radiolabel [Al^{18}F]NODA-MPAA-HTA using a simple reaction mixture of 100 μL of ^{18}F solution and acetonitrile in the presence of $AlCl_3$ stock solution (pH 3–5), and the reaction to incorporate gentisic acid as an antioxidant excipient in the radiopharmaceutical formulation was carried out under heating conditions at temperatures ranging from 70 to 140 °C for a duration of 5 to 20 min. This heating process allows for the proper incorporation of gentisic acid into the formulation, ensuring its stabilizing effects on the active ingredients and preventing radiation self-decomposition. The reaction was carried out under heating at 70–140 °C for 5–20 min. The results of monitoring pH, reaction temperature and time (Fig.1) confirmed that the radioiodination method was dependent on pH, temperature and time. The optimal reaction conditions were pH 4, 110 °C and 20 min. The detailed reaction system is shown in Supplemental, Table 1.

The radiochemical yield of [Al^{18}F]NODA-MPAA-HTA was 60 %−80 % (non-decay corrected) and radiochemical purity over 95 % after C18 column purification. The radio-HPLC analysis results (Supplemental Fig. 2) revealed that the retention time of [Al^{18}F]NODA-MPAA-HTA was 10.87 min, consistent with that of the precursor (TR = 10.06 min). The molar activity was calculated as 122 GBq/μmol based on radioactivity and the ultraviolet peak in the HPLC chromatogram. The log *P* value was −1.42 ± 0.03 indicating hydrophilicity for in vivo applications. The total time of radiosynthesis was within 30 min, including the radiolabeling and purification processes. These positive results suggested that this method can provide a highly efficient and convenient approach for producing [Al^{18}F]NODA-MPAA-HTA for PET imaging applications.

4.2. Characterization of [Al^{18}F]NODA-MPAA-HTA

The stability of [Al^{18}F]NODA-MPAA-HTA in saline and bovine serum (37 °C, 2 h) was shown in Fig. 2. The radiochemical purity of [Al^{18}F]NODA-MPAA-HTA in two systems was more than 95 %. Only the main peak of [Al^{18}F]NODA-MPAA-HTA was obviously observed on the HPLC chromatogram, indicating that [Al^{18}F]NODA-MPAA-HTA had good stability in vitro. This finding suggested that the radiotracer can withstand potential challenges during transportation, storage, and preparation, and may be a reliable choice for PET imaging applications in vivo.

Table 1
Major pharmacokinetics parameters in the blood derived by non-atrioventricular model modeling after i.v. administration of [Al^{18}F]NODA-MPAA-HTA at 185 MBq/kg in healthy mice within 2 h p.i.. ($n = 3$).

Parameter	Unit	Value
$AUC_{(0\text{-}t)}$	%ID/g·min	634.27 ± 213.37
$AUC_{(0\text{-}\infty)}$	%ID/g·min	1146.99 ± 593.97
$t_{1/2z}$	min	37.63 ± 13.05
T_{max}	min	10.00 ± 0.00
C_{max}	%ID/g	13.66 ± 5.04
CLz	L/h	0.026 ± 0.01
Vd	L	1.37 ± 0.41

$AUC_{(0-t)}$ and $AUC_{(0-\infty)}$: area under the curve. $t_{1/2z}$: elimination half-life. T_{max}: peak time. C_{max}: peak concentration. CLz: clearance. Vd: volume of distribution. The values are expressed as mean ± SD.

4.3. Pharmacokinetics

The time-activity curve of blood after i.v. of [Al^{18}F]NODA-MPAA-HTA into normal BALB/c mice was shown in Fig. 3. The blood elimination half-life of [Al^{18}F]NODA-MPAA-HTA was 37.63 ± 13.05 min, indicating moderate clearance from circulation that may be advantageous for early PET imaging of NETs. Major pharmacokinetics parameters were summarized in Table 1. These results suggested that our radiotracer has favorable properties for potential clinical translation as a diagnostic tool for NETs.

4.4. Saturation cell binding and cellular uptake

The cell binding studies of [Al^{18}F]NODA-MPAA-HTA were performed in SSTR2(+) HEK293-SSTR2 cells to give the saturated binding curves (Fig. 4). The affinity of [Al^{18}F]NODA-MPAA-HTA (K_d = 8.77 ± 1.14 nM, $n = 4$) was equivalent than [^{68}Ga]Ga-DOTA-TATE (K_d = 7.36 ± 1.02 nM), as reported (Xie et al., 2021). Saturated binding experiments revealed a nanomolar inhibition potency toward SSTR2.

SSTR2(+) HEK293-SSTR2 cells were exposed to [Al^{18}F]NODA-MPAA-HTA, and at selected time points the amount of uptaked was determined (Fig. 4). Uptake increased with incubation time and stabilized after about 60 min (12.11 ± 0.32 %).The radioactivity of cell uptake was significantly blocked (5.20 ± 0.28 %) by the addition of NODA-MPAA-HTA peptide ($p < 0.001$), indicating its high specificity for SSTR2.

4.5. PET imaging studies

For PET/CT study, tumor-bearing mice were intravenously injected with 5 MBq [Al^{18}F]NODA-MPAA-HTA in 125 μL saline. As shown in

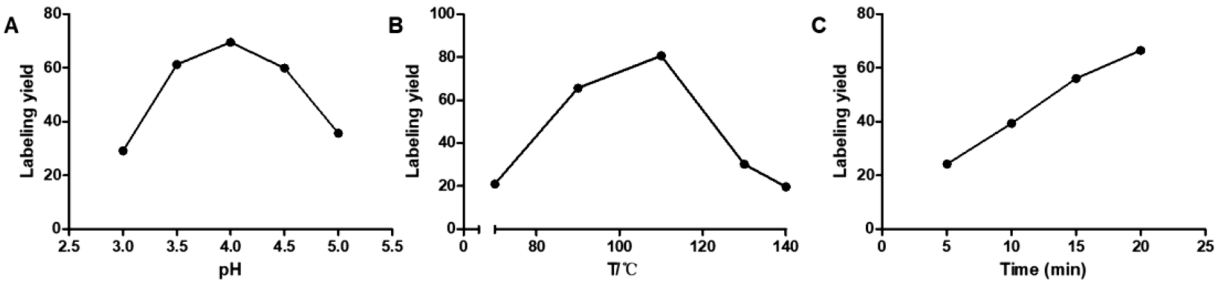

Fig. 1. Effect of pH (A), reaction temperature (B) and reaction time (C) on labeling efficiency.

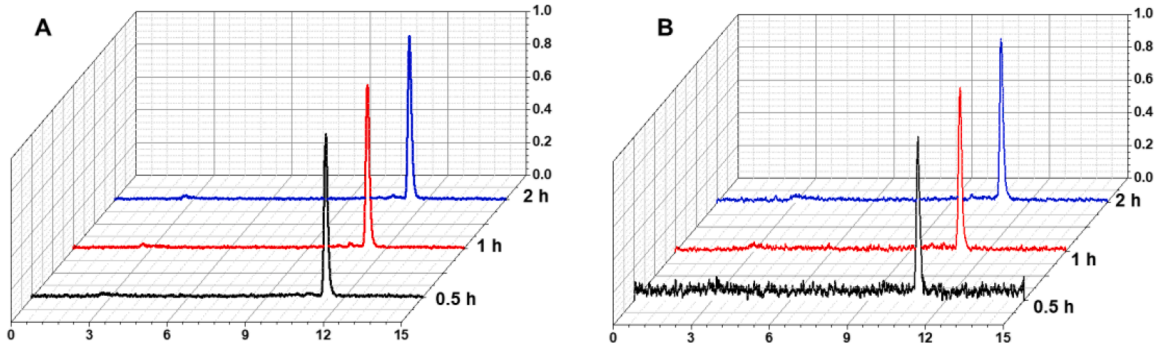

Fig. 2. HPLC profiles of [Al^{18}F]NODA-MPAA-HTA after in vitro incubation in saline (A) and bovine serum (B) for 2 h.

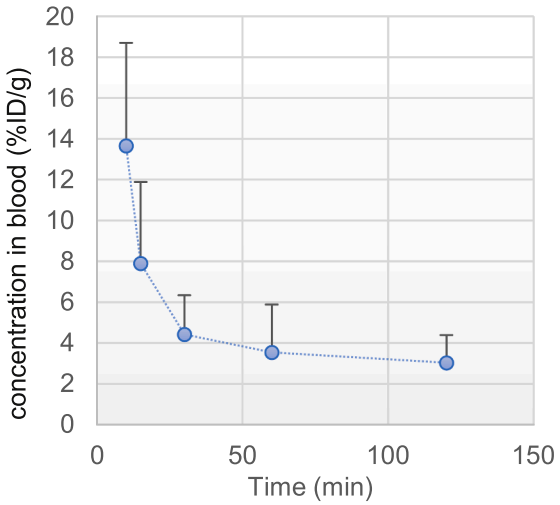

Fig. 3. Time-activity curve of [Al^{18}F]NODA-MPAA-HTA in the blood of healthy BALB/c mice. Data are expressed as mean ± SD (n = 3).

Fig. 5, the implanted HEK293-SSTR2 tumors into the right shoulder of nude mice were clearly visualized. And the tumor uptakes were quantified as 6.90 ± 2.40, 7.14 ± 2.73 and 6.58 ± 2.20%ID/g at 0.5 h, 1 h and 2 h, respectively. The tumor uptakes at available time points were 5 - 6 folds over the muscle uptakes, indicating good image contrast (all p values < 0.05). However, it should be noted that accumulation of the radiotracer was also observed in the liver and kidney, consistent with the distribution pattern observed in our previous studies. These findings suggest that [Al^{18}F]NODA-MPAA-HTA has potential as a PET imaging agent for tumors, but further investigations are needed to fully understand the factors influencing its biodistribution and clearance in vivo.

Furthermore, representative PET images obtained at 0.5 h p.i. of [Al^{18}F]NODA-MPAA-HTA in HEK293-SSTR2 tumor-bearing mice, and with excessive of precursor for blocking, as shown in Fig. 6. Quantitative tumor uptakes and tumor-to-muscle ratios was accessed from above images (Fig. 7). The results showed that the radioactive uptake of the tumor site after inhibition was significantly reduced, with an uptake value of 1.62 ± 0.58 % ID/g. The tumor uptake was basically consistent with the background value, indicating that the uptake mechanism of [Al^{18}F]NODA-MPAA-HTA was mediated by SSTR.

In addition, the most important concern was the relatively low bone uptake, which was 1.54 ± 0.43, 1.43 ± 0.63 and 1.08 ± 0.34 % ID/g for 0.5 h, 1 h and 2 h respectively, indicating that defluorination did not occur in vivo. which is a common issue with some radiotracers and can lead to high bone uptake and poor image quality.

4.6. *Biodistribution of [Al^{18}F]NODA-MPAA-HTA*

Biodistribution results of [Al^{18}F]NODA-MPAA-HTA were shown in Fig. 8. The radioactivity uptakes in the tumor were 14.27 ± 5.31, 20.49 ± 12.54 and 28.83 ± 11.70% ID/g for 0.5 h, 1 h and 2 h, respectively. Obviously, these results were higher than those from the PET imaging study, possibly due to differences in the two experimental methods. Specifically, the range of region of interest (ROI) delineated in PET imaging includes areas with lower uptake, resulting in a lower calculated average uptake. Additionally, the disparity in specific activity between the two experiments may also contribute to this variation.

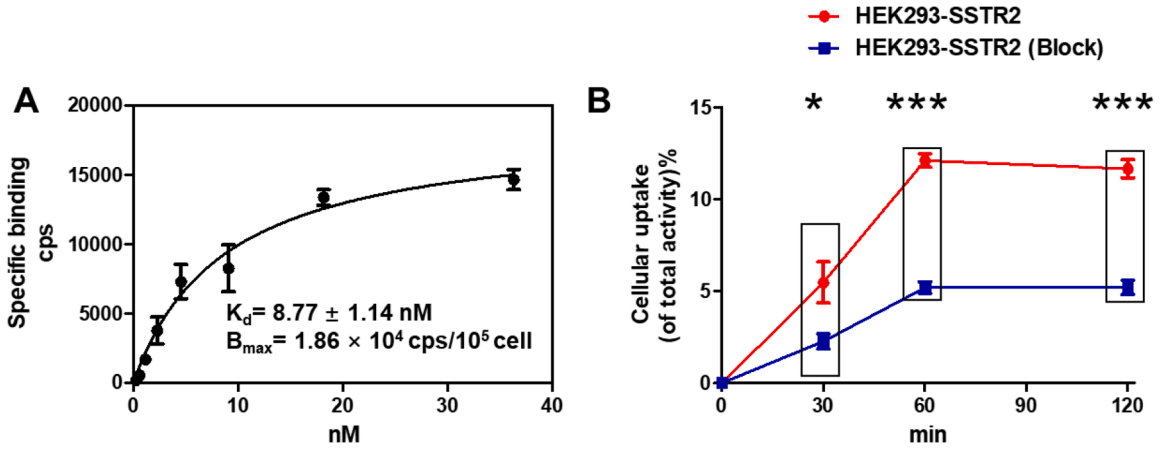

Fig. 4. The saturation cell binding (A) and cellular uptake (B) study of [Al^{18}F]NODA-MPAA-HTA.

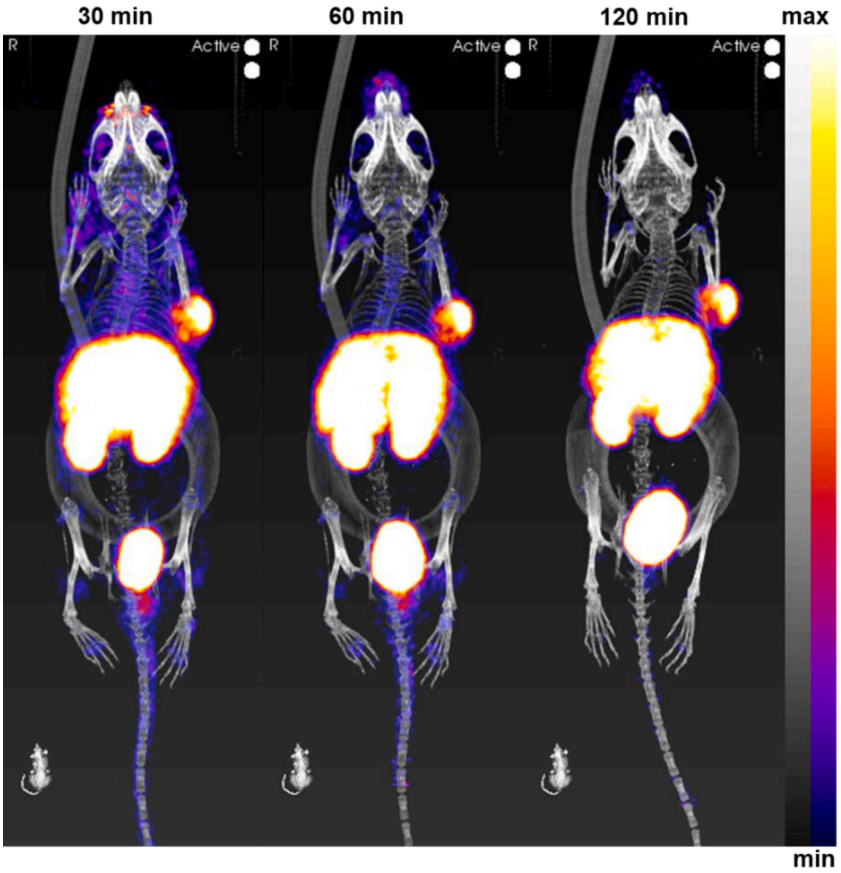

Fig. 5. Representative PET images obtained at 0.5, 1 and 2 h p.i. of [Al^{18}F]NODA-MPAA-HTA in HEK293-SSTR2 tumor-bearing mice.

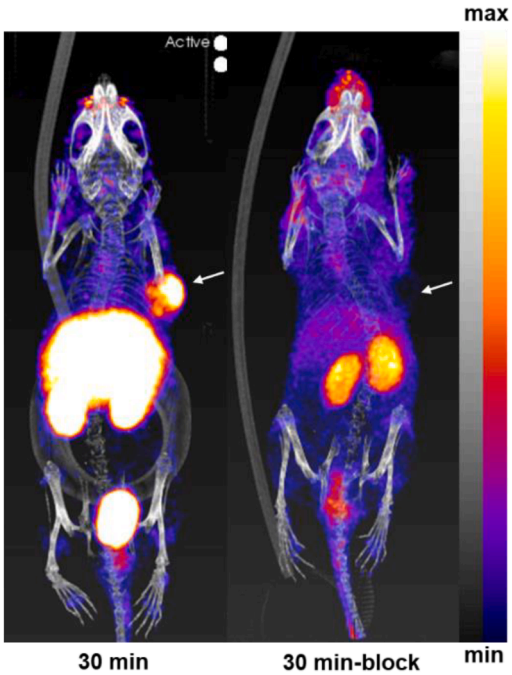

Fig. 6. Representative PET images obtained at 0.5 h p.i. of [Al^{18}F]NODA-MPAA-HTA in HEK293-SSTR2 tumor-bearing mice, and with excessive of precursor for blocking. Quantitative tumor uptakes and tumor-to-muscle ratios were accessed from above images (the white arrow indicates tumor suppression).

5. Discussion and conclusions

As a new somatostatin analogue, the KE108 peptide has been developed to increase tumor responsiveness by activating multiple SSTR subtypes (Cescato et al., 2010). The [Al^{18}F]NODA-MPAA-HTA probe designed and synthesized through chemical modification has excellent biological targeting ability. The approximately 30 min [Al^{18}F]NODA-MPAA-HTA blood elimination half-life was relatively suitable for the ^{18}F half-life, suggesting that the radiolabeling does not remain for an extended period to reduce non-characteristic damage.

The biodistribution and PET imaging results revealed that the liver and kidney may serve as the primary elimination route for [Al^{18}F]NODA-MPAA-HTA. The low uptake in bone suggests high metabolic stability, as freely circulating ^{18}F-fluoride would cause bone toxicity. Notably, when compared to ^{68}Ga-octreotide derivatives with high affinity to SSTR, such as ^{68}Ga-Dotatate, [Al^{18}F]NODA-MPAA-HTA had similar tumor uptake and contrast ratio.

These encouraging preclinical experimental findings represent an important step towards the clinical implementation of PET imaging. The targeting ability of [Al^{18}F]NODA-MPAA-HTA to SSTR has been verified through a series of in vivo and in vitro bio-evaluation, and further studies are needed to determine the safety and optimal dose for SSTR-positive NETs imaging. Subsequent later-phase studies are required to validate these initial findings and to evaluate the clinical efficacy and safety of [Al^{18}F]NODA-MPAA-HTA in other tumor models Nevertheless, the results of this study provide promising evidence for the development of novel radiotracers using the one-step ^{18}F-AlF labeling method for the diagnosis and management of neuroendocrine tumors.

Declaration of Competing Interest

The authors declare that they have no known competing financial

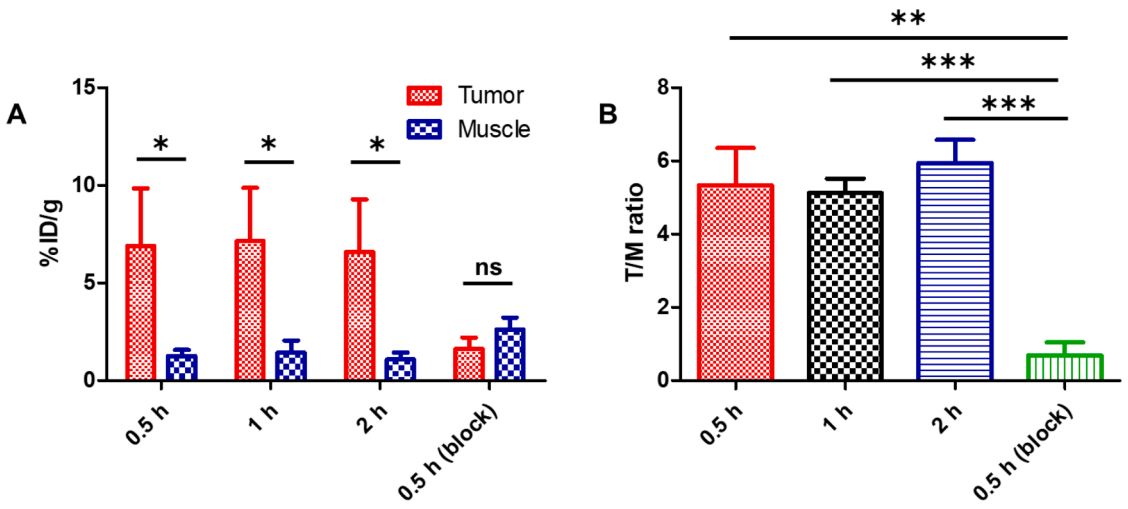

Fig. 7. Quantitative tumor and muscle uptakes (A) and tumor-to-muscle ratios (B).

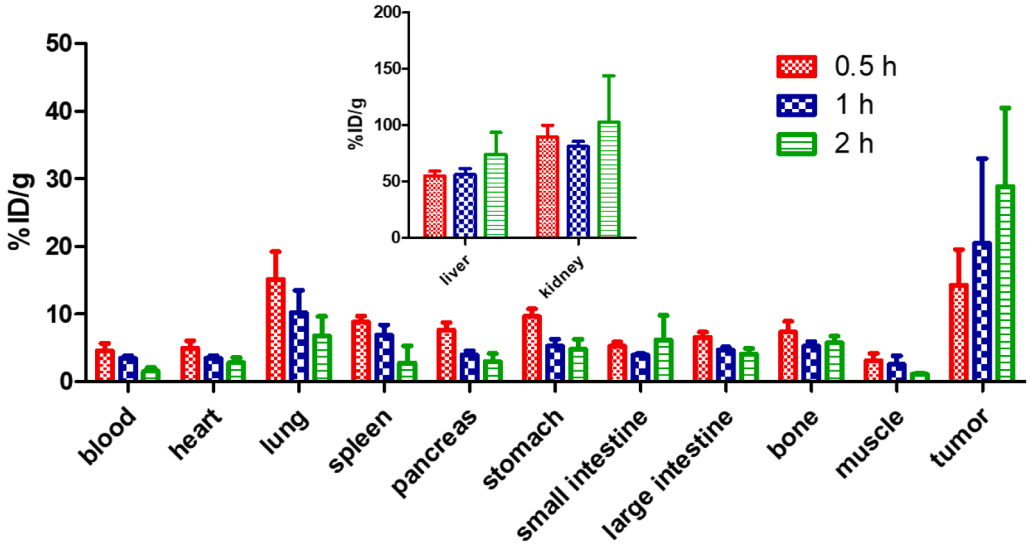

Fig. 8. Biodistribution of [Al^{18}F]NODA-MPAA-HTA in HEK293-SSTR2 tumor-bearing mice.

interests or personal relationships that could have appeared to influence the work reported in this paper.

Data availability

Data will be made available on request.

Acknowledgements

The Young Talents Program of China National Nuclear Corporation (No.20180821-GK009). Thanks to Dr Guo Feihu for his early guidance on the program.

Supplementary materials

Supplementary material associated with this article can be found, in the online version, at doi:10.1016/j.ejps.2023.106671.

References

André, João P, Mäcke, Helmut, Kaspar, A., 2002. In vivo and in vitro ^{27}Al NMR studies of aluminum(III) chelates of triazacyclononane polycarboxylate ligands. J. Inorg. Biochem. 88 (1), 1–6. https://doi.org/10.1016/S0162-0134(01)00340-3.

Cai, Z., Ouyang, Q., Zeng, D., Nguyen, K.N., Modi, J., Wang, L., White, A.G., Rogers, B.E., Xie, X.Q., Anderson, C.J., 2014. ^{64}Cu-labeled somatostatin analogues conjugated with cross-bridged phosphonate-based chelators via strain-promoted click chemistry for PET imaging: in silico through in vivo studies. J. Med. Chem. 57, 6019–6029. https://doi.org/10.1021/jm500416f.

Campana, D., Ambrosini, V., Pezzilli, R., Fanti, S., Labate, A.M., Santini, D., Ceccarelli, C., Nori, F., Franchi, R., Corinaldesi, R., Tomassetti, P., 2010. Standardized uptake values of ^{68}Ga-DOTANOC PET: a promising prognostic tool in neuroendocrine tumors. J. Nucl. Med. 51, 353–359. https://doi.org/10.2967/jnumed.109.066662.

Capello, A., Krenning, E.P., Breeman, W., Bernard, B.F., Jong, M., 2003. Radiopharmaceuticals, Tyr$_3$-octreotide and Tyr$_3$-octreotate radiolabeled with ^{177}Lu or ^{90}Y: peptide receptor radionuclide therapy results in vitro. J. Cancer Biotherapy 18, 761. https://doi.org/10.1089/108497803770418300.

Cescato, R., Loesch, K.A., Waser, B., Macke, H.R., Rivier, J.E., Reubi, J.C., Schonbrunn, A., 2010. Agonist-biased signaling at the sst2A receptor: the multi-somatostatin analogs KE108 and SOM230 activate and antagonize distinct signaling pathways. Mol. Endocrinol. 24, 240–249. https://doi.org/10.1210/me.2009-0321.

Chen, G., Jaskula–Sztul, R., Harrison, A., Dammalapati, A., Xu, W., Cheng, Y., Chen, H., Gong, S., 2016. KE108-conjugated unimolecular micelles loaded with a novel HDAC inhibitor thailandepsin-A for targeted neuroendocrine cancer therapy. Biomaterials 97, 22–33. https://doi.org/10.1016/j.biomaterials.2016.04.029.

Chen, X., Zhang, Q., Zhang, Y., Fang, J., Jiang, D., Mou, Z., Liu, H., Su, R., Wang, C., He, F., Chen, X., Xie, F., Pan, X., Li, Z., 2021. ^{18}F-Labelled pyrrolopyrimidines reveal brain leucine-rich repeat kinase 2 expression implicated in Parkinson's disease. Eur. J. Med. Chem. 214, 113245 https://doi.org/10.1016/j.ejmech.2021.113245.

Dasari, A., Shen, C., Halperin, D., Zhao, B., Zhou, S., Xu, Y., Shih, T., Yao, J.C., 2017. Trends in the incidence, prevalence, and survival outcomes in patients with neuroendocrine tumors in the united states. JAMA Oncol. 3, 1335–1342. https://doi.org/10.1001/jamaoncol.2017.0589.

Edit, Farkas, Tamás, et al., 2015. Equilibrium and dissociation kinetics of the [Al(NOTA)] complex (NOTA = 1,4,7-triazacyclononane-1,4,7-triacetate). Reaction Kinetics Mech. Catal. https://doi.org/10.1007/s11144-015-0892-6.

Eisenwiener, K.P., Prata, M., Buschmann, I., Zhang, H.W., Santos, A.C., Wenger, S., Reubi, J.C., Mäcke, H.R., 2002. NODAGATOC, a new chelator-coupled somatostatin analogue labeled with [$^{67/68}$Ga] and [^{111}In] for SPECT, PET, and targeted therapeutic applications of somatostatin receptor (hsst2) expressing tumors. Bioconjugate Chem. 13, 530–541. https://doi.org/10.1021/bc010074f.

Ginj, M., Zhang, H., Eisenwiener, K.P., Wild, D., Schulz, S., Rink, H., Cescato, R., Reubi, J.C., Maecke, H.R., 2008. New pansomatostatin ligands and their chelated versions: affinity profile, agonist activity, internalization, and tumor targeting. J. Clin. Cancer Res. 14 https://doi.org/10.1158/1078-0432.CCR-07-1687.

Hallet, J., Law, C.H.L., Cukier, M., Saskin, R., Liu, N., Singh, S., 2015. Exploring the rising incidence of neuroendocrine tumors: a population-based analysis of epidemiology, metastatic presentation, and outcomes. Cancer 121, 589–597. https://doi.org/10.1002/cncr.29099.

Hofmann, M., Maecke, H., Börner, R., Weckesser, E., Schöffski, P., 2001. Biokinetics and imaging with the somatostatin receptor PET radioligand ^{68}Ga-DOTATOC: preliminary data. Eur. J. Nucl. Med. Mol. Imaging. https://doi.org/10.1007/s002590100639.

Kaemmerer, D., Peter, L., Lupp, A., Schulz, S., Sanger, J., Prasad, V., Kulkarni, H., Haugvik, S.P., Hommann, M., Baum, R.P., 2011. Molecular imaging with ^{68}Ga-SSTR PET/CT and correlation to immunohistochemistry of somatostatin receptors in neuroendocrine tumours. Eur. J. Nucl. Med. Mol. Imaging 38, 1659–1668. https://doi.org/10.1007/s00259-011-1846-5.

Kjaer, A., Knigge, U., 2015. Use of radioactive substances in diagnosis and treatment of neuroendocrine tumors. J. Scand. Gastro 50, 740–747. https://doi.org/10.3109/00365521.2015.1033454.

Kobayashi, N., Takano, S., Ito, K., Sugiura, M., Ogawa, M., Takeda, Y., Okubo, N., Suzuki, A., Tokuhisa, M., Kaneta, T., Utsunomiya, D., Hata, M., Inoue, T., Hosono, M., Kinuya, S., Ichikawa, Y., 2021. Safety and efficacy of peptide receptor radionuclide therapy with ^{177}Lu-DOTA^{0}-Tyr^{3}-octreotate in combination with amino acid solution infusion in Japanese patients with somatostatin receptor-positive, progressive neuroendocrine tumors. Ann. Nucl. Med. 35, 1332–1341. https://doi.org/10.1007/S12149-021-01674-9.

Kourie, H.R., 2016. Digestive neuroendocrine tumor distribution and characteristics according to the 2010 who classification: a single institution experience in Lebanon. J. Asian Pac. Cancer P 17, 2679. https://doi.org/10.7314/APJCP.2016.17.5.2679.

Kumar, K., 2018. ^{18}F-AlF-labeled biomolecule conjugates as imaging pharmaceuticals. J. Nucl. Med. 59, 1208–1209. https://doi.org/10.2967/jnumed.118.210609.

Kunikowska, J., Krolicki, L., Hubalewska-Dydejczyk, A., Mikolajczak, R., Sowa-Staszczak, A., Pawlak, D., 2011. Clinical results of radionuclide therapy of neuroendocrine tumours with ^{90}Y-DOTATATE and tandem ^{90}Y/^{177}Lu-DOTATATE: which is a better therapy option. Eur. J. Nucl. Med. Mol. Imaging 38, 1788–1797. https://doi.org/10.1007/s00259-011-1833-x.

Leupe, H., Ahenkorah, S., Dekervel, J., Unterrainer, M., Van Cutsem, E., Verslype, C., Cleeren, F., Deroose, C.M., 2023. ^{18}F-labeled somatostatin analogs as PET tracers for the somatostatin receptor: ready for clinical use. J. Nucl. Med. https://doi.org/10.2967/jnumed.123.265622.

Lewis, J.S., Lewis, M.R., Srinivasan, A., Schmidt, M.A., Wang, J., Anderson, C.J., 1999. Comparison of four ^{64}Cu-labeled somatostatin analogues in vitro and in a tumor-bearing rat model: evaluation of new derivatives for positron emission tomography imaging and targeted radiotherapy. J. Med. Chem. 42, 1341–1347. https://doi.org/10.1021/jm980602h.

Loft, Annika, Knigge, Ulrich, Langer, Seppo, Oturai, W., Peter, Kjaer, 2017. Head-to-head comparison of Cu-64-DOTATATE and Ga-68-DOTATOC PET/CT: a prospective study of 59 patients with neuroendocrine Tumors. J. Nucl. Med. (3) https://doi.org/10.2967/jnumed.116.180430. .DOI.

Malik, N., Baur, B., Winter, G., Reske, S.N., Beer, A.J., Solbach, C., 2015. Radiofluorination of PSMA-HBED via Al^{18}F^{2+} chelation and biological evaluations in vitro. Mol. Imaging Biol. 17, 777–785. https://doi.org/10.1007/s11307-015-0844-6.

Martell, A., 1996. Coordination of Al(III) in the environment and in biological systems. Coord. Chem. Rev. https://doi.org/10.1016/0010-8545(95)01228-1.

Mcbride, W.J., D'Souza, C.A., Sharkey, R.M., Karacay, H., Goldenberg, D.M.J.B.C., 2010. Improved ^{18}F labeling of peptides with a fluoride-aluminum-chelate complex. Bioconjugate Chem. 21, 1331. https://doi.org/10.1021/bc100137x.

McBride, W.J., Sharkey, R.M., Karacay, H., D'Souza, C.A., Rossi, E.A., Laverman, P., Chang, C.H., Boerman, O.C., Goldenberg, D.M., 2009. A novel method of ^{18}F radiolabeling for PET. J. Nucl. Med. 50, 991–998. https://doi.org/10.2967/jnumed.108.060418.

Modlin, I.M., Pavel, M., Kidd, M., Gustafsson, B.I., 2010. Review article: somatostatin analogues in the treatment of gastroenteropancreatic neuroendocrine (carcinoid) tumours. Aliment. Pharmacol. Ther. 31, 169–188. https://doi.org/10.1111/j.1365-2036.2009.04174.x.

Reubi, J.C., Maecke, H.R., 2008. Peptide-based probes for cancer imaging. J. Nucl. Med. 49, 1735–1738. https://doi.org/10.2967/jnumed.108.053041.

Strosberg, J., Elhaddad, G., Wolin, E., Hendifar, A., Yao, J., Chasen, B., Mittra, E., Kunz, P.L., Kulke, M.H., Jacene, H., 2017. Phase 3 Trial of Lu-177-dotatate for midgut neuroendocrine tumors. N. Engl. J. Med. 376 (2), 125–135. https://doi.org/10.1056/NEJMoa1607427.

Toshihiko, M., Tetsuhide, I., Izumi, K., Shinji, U., JNETS Project Study Group, 2020. Recent epidemiology of patients with gastro-entero-pancreatic neuroendocrine neoplasms (GEP-NEN) in Japan: a population-based study. J. BMC Cancer 20 (1), 1104. https://doi.org/10.1186/s12885-020-07581-y.

Turaga, K.K., Kvols, L.K., 2011. Recent progress in the understanding, diagnosis, and treatment of gastroenteropancreatic neuroendocrine tumors. CA Cancer J. Clin. 61, 113–132. https://doi.org/10.3322/caac.20097.

Wild, D., Schmitt, J.R., Ginj, M., M?Cke, H., Bernard, B., Krenning, E., Jong, M., Wenger, S., Reubi, J.C., 2003. DOTA-NOC, a high-affinity ligand of somatostatin receptor subtypes 2, 3 and 5 for labelling with various radiometals. J. Eur. Nucl. Med. Mol. I 30, 1338–1347. https://doi.org/10.1016/j.colsurfa.2008.02.036.

Xie, Q., Liu, T., Ding, J., Zhou, N., Meng, X., Zhu, H., Li, N., Yu, J., Yang, Z., 2021. Synthesis, preclinical evaluation, and a pilot clinical imaging study of [^{18}F]AlF-NOTA-JR11 for neuroendocrine neoplasms compared with [^{68}Ga]Ga-DOTA-TATE. Eur. J. Nucl. Med. Mol. Imaging 48, 3129–3140. https://doi.org/10.1007/s00259-021-05249-8.

Yao, J.C., Hassan, M., Phan, A., Dagohoy, C., Leary, C., Mares, J.E., Abdalla, E.K., Fleming, J.B., Vauthey, J.N., Rashid, A., Evans, D.B., 2008. One hundred years after "carcinoid": epidemiology of and prognostic factors for neuroendocrine tumors in 35,825 cases in the United States. J. Clin. Oncol. 26, 3063–3072. https://doi.org/10.1200/JCO.2007.15.4377.